THE JOURNAL OF BIOLOGICAL CHEMISTRY VOL. 282, NO. 22, pp. 16288–16294, June 1, 2007

Crystal Structures and Site-directed Mutagenesis of a Mycothiol-dependent Enzyme Reveal a Novel Folding and Molecular Basis for Mycothiol-mediated Maleylpyruvate Isomerization*[S]

Received for publication, November 6, 2006, and in revised form, March 30, 2007 Published, JBC Papers in Press, April 11, 2007, DOI 10.1074/jbc.M610347200

Rui Wang[‡§1], Ya-Jie Yin[§¶1], Feng Wang[‡], Mei Li[‡§], Jie Feng[¶], Hong-Mei Zhang[‡], Ji-Ping Zhang[‡], Shuang-Jiang Liu[¶2], and Wen-Rui Chang[‡3]

From the [‡]National Laboratory of Biomacromolecules, Institute of Biophysics, Chinese Academy of Sciences, Beijing 100101, the [¶]State Key Laboratory of Microbial Resource, Institute of Microbiology, Chinese Academy of Sciences, Beijing 100080, and the [§]Graduate University of Chinese Academy of Sciences, Beijing 100049, China

Mycothiol (MSH) is the major low molecular mass thiols in many Gram-positive bacteria such as *Mycobacterium tuberculosis* and *Corynebacterium glutamicum*. The physiological roles of MSH are believed to be equivalent to those of GSH in Gram-negative bacteria, but current knowledge of MSH is limited to detoxification of alkalating chemicals and protection from host cell defense/killing systems. Recently, an MSH-dependent maleylpyruvate isomerase (MDMPI) was discovered from *C. glutamicum*, and this isomerase represents one example of many putative MSH-dependent enzymes that take MSH as cofactor. In this report, fourteen mutants of MDMPI were generated. The wild type and mutant (H52A) MDMPIs were crystallized and their structures were solved at 1.75 and 2.05 Å resolution, respectively. The crystal structures reveal that this enzyme contains a divalent metal-binding domain and a C-terminal domain possessing a novel folding pattern ($\alpha\beta\alpha\beta\beta\alpha$ fold). The divalent metal-binding site is composed of residues His[52], Glu[144], and His[148] and is located at the bottom of a surface pocket. Combining the structural and site-directed mutagenesis studies, it is proposed that this surface pocket including the metal ion and MSH moiety formed the putative catalytic center.

Mycothiol, also known as MSH[4] and chemically 1D-*myo*-inosityl-2-(*N*-acetyl-L-cysteinyl)-amido-2-deoxy-α-D-glucopyranoiside (1–4), is the major low molecule mass thiol in many groups of Gram-positive bacteria such as coryneform bacteria, mycobacteria, and streptomycetes (5, 6). These bacteria synthesize MSH but lack GSH molecule that plays important roles in many physiological processes. It is believed that MSH functions similarly to GSH in many microbial activities (6). However, the understanding of MSH physiological function was limited to detoxification of reactive oxygen/alkalating species and to protection of pathogens such as *Mycobacterium tuberculosis* from host cell defense systems (1, 7, 8). Very recently, a novel physiological role of MSH in assimilation of aromatic compounds was described and an MSH-dependent maleylpyruvate isomerase (MDMPI) was identified in *Corynebacterium glutamicum* (9). This MDMPI catalyzes the conversion of maleylpyruvate (substrate) to fumarylpyruvate (product) (Fig. 1).

BLAST searches with MDMPI sequence against GenBank™ and other protein data bases revealed that MDMPI is not homologous to any functionally identified proteins but showed significant identities (27–36%) to a range of conserved hypothetical proteins from the genomes of *Streptomyces coelicolor*, *Streptomyces avermitilis*, *Propionibacterium acnes*, and *Nocardia farcinica* (10) (Fig. 2*A*). Earlier research on mycothiol biochemistry and biosynthesis has been conducted with mycobacteria such as *M. tuberculosis*, with the ultimate aim of defining new targets against tuberculosis, the resurgence of which has been a growing health concern in both developed and developing nations. The understanding of MSH-dependent enzyme structure is the key to the characterization of MSH-dependent enzymes that are helpful for the development of new drugs against diseases caused by *Mycobacterium* spp.

To elucidate the catalytic mechanism of MDMPI and to provide clues to find more MSH-dependent enzymes, we have determined the crystal structure of MDMPI from *C. glutamicum* at a resolution of 1.75Å. The structure reveals that the MDMPI contains two domains: A metal binding domain binds a divalent metal cofactor (Zn^{2+}) and an extended domain con-

* This work was supported by National Natural Sciences Foundation of China and Knowledge Innovation Program of the Chinese Academy of Sciences. The costs of publication of this article were defrayed in part by the payment of page charges. This article must therefore be hereby marked "*advertisement*" in accordance with 18 U.S.C. Section 1734 solely to indicate this fact.

[S] The on-line version of this article (available at http://www.jbc.org) contains supplemental Tables S1 and S2.

The atomic coordinates and structure factors (code 2NSF and 2NSG) have been deposited in the Protein Data Bank, Research Collaboratory for Structural Bioinformatics, Rutgers University, New Brunswick, NJ (http://www.rcsb.org/).

[1] These two authors contributed equally to this work. R. W. contributed to the crystallization and structure determination and analysis, and Y.-J. Y. contributed to the mutagenesis and enzymatic activity determination.

[2] To whom correspondence may be addressed: Institute of Microbiology, Chinese Academy of Sciences, ZhongGuanCun, Haidian, Beijing 100080, China. Tel.: 86-10-62527118; Fax: 86-10-62652317; E-mail: liusj@sun.im.ac.cn.

[3] To whom correspondence may be addressed: National Laboratory of Biomacromolecules, Institute of Biophysics, Chinese Academy of Sciences, 15 Datun Rd., Chaoyang District, Beijing 100101, China. Tel.: 86-10-64888512; Fax: 86-10-64889867; E-mail: wrchang@sun5.ibp.ac.cn.

[4] The abbreviations used are: MSH, mycothiol; MDMPI, MSH-dependent maleylpyruvate isomerase.

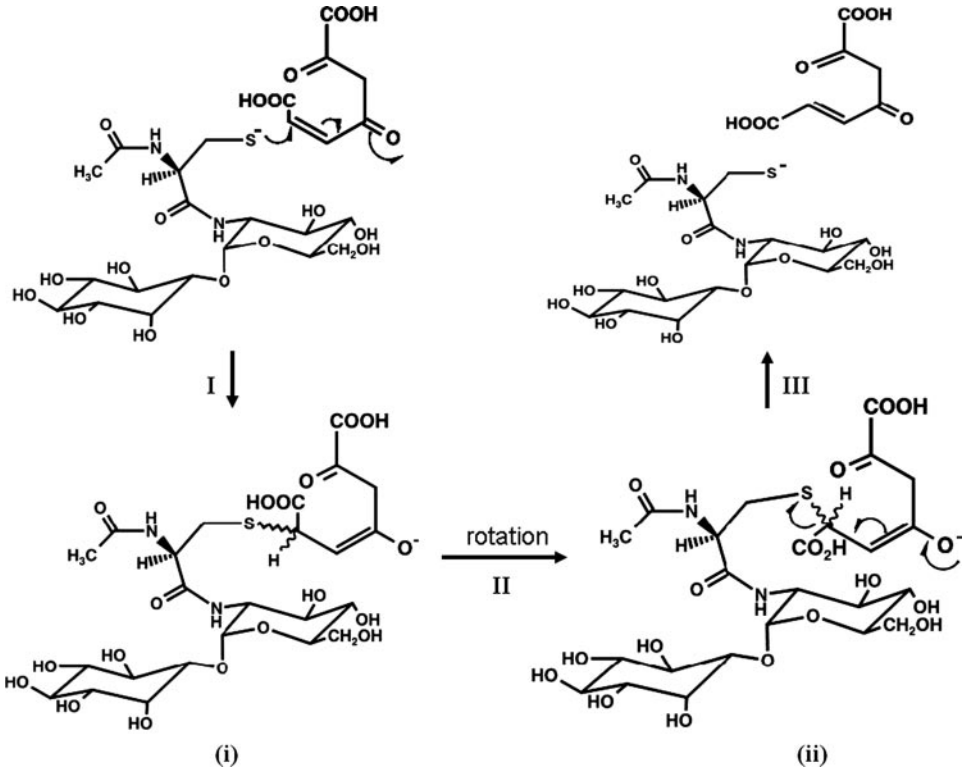

FIGURE 1. **Isomerization of maleylpyruvate into fumarylpyruvate catalyzed by mycothiol-dependent maleylpyruvate isomerase.** Intermediates *(i)* and *(ii)* have not been experimentally confirmed.

tains totally new folding. The site-directed mutagenesis reveals 9 of the 14 conserved amino acid residues are essential for activity. One mutant (H52A) was crystallized. By combination of structural and biochemical results, a putative catalytic center is proposed. So far as we know this is the first structure of an MSH-dependent enzyme, as well as an enzyme involved in gentisate/3-hydroxybenzoate assimilation that is widely existed in bacteria and participate in microbial geocycling of elements of aromatic compounds in nature.

EXPERIMENTAL PROCEDURES

Bacterial Strains, Plasmids, and Culture Conditions—Bacterial strains and plasmids used in this study are listed in supplemental Table S1. *Escherichia coli* strains were grown aerobically on a rotary shaker (150 rpm) at 37 °C in LB broth or on LB plate with 1.5% (w/v) agar. When needed, kanamycin at 50 μg ml^{-1} for *E. coli* was used.

Expression and Purification of MDMPI and Its Mutants—Various derivatives of plasmid pET28a (supplemental Table S1) that harbor MDMPI or its mutants were constructed by methods described previously (10). Recombinant proteins were expressed in *E. coli* BL21 (DE3) cells by inducing with 0.5 mM isopropyl-1-thio-β-D-galactopyranoside when the culture reached an A_{600} of 0.6–0.8. The culture was harvested after growing for additional 8 h at 25 °C. Protein was purified using a nickel affinity column and a Superdex 75 gel-filtration column (GE Healthcare). The prepared protein sample was checked for purity by SDS-PAGE and by gel-filtration chromatography, which showed only one protein of 28 kDa corresponding to the molecular mass of MDMPI and its mutants. After changing buffer to 10 mM Tris (pH 8.0) by repeatedly concentration and dilution using Amicon Ultra-4 concentrators (molecular weight cutoff 5000), the purified protein was finally concentrated to 17 mg/ml and stored at −80 °C.

Crystallization and Data Collection—The hanging-drop vapor-diffusion method was used for crystallization. The drop was formed by mixing 1 μl of protein solution (17 mg/ml) with an equal volume of reservoir solution containing 1.2 M $(NH_4)_2SO_4$, 12% glycerol, and 0.1 M Tris (pH 8.5). A 1.75 Å resolution native data set was collected utilizing Rigaku RAXIS IV image plate detector at Institute of Biophysics (Chinese Academy of Sciences). A bromide derivative was prepared by soaking the crystal in cryoprotecting solution containing 1.2 M $(NH_4)_2SO_4$, 25% glycerol, 1 M NaBr, and 0.1 M Tris (pH 8.5) for 10 min. Single-wavelength anomalous dispersion data were collected at the Beijing Synchrotron Radiation Facility at the peak wavelength of bromine (0.920 Å) with 1° oscillation and an exposure of 15 s per image. A total of 600° of data were collected to a resolution of 1.95 Å with an average of 20-fold redundancy.

The crystallization of mutant H52A was performed similarly to that of native MDMPI. The drops were composed of 1 μl of protein solution (15 mg/ml) and 1 μl of reservoir solution containing 1.4 M $(NH_4)_2SO_4$, 11% glycerol, and 0.1 M Tris (pH 8.5). A 2.05 Å resolution data set for this mutant was collected at the Institute of Biophysics (Chinese Academy of Sciences).

All the diffraction data (Table 1) were integrated using DENZO and scaled using SCALEPACK (11).

Phasing, Structural Determination, Refinement, and Analysis—Five bromide heavy atom sites in the asymmetric unit were determined using PHENIX via the single-wavelength anomalous dispersion method (12, 13). After phase improvement an initial model was built using PHENIX with the final figure of merit 0.65 for eight bromide sites. ARP/wARP was used to automated model rebuilding with the sequence of MDMPI (14, 15). The model was subsequently subjected to annealing refinement by CNS (16) using 50-1.75 Å data, and the traditional crystallographic refinement was carried out using CNS (16). After several cycles of refinement and model rebuilding a final model with an R factor of 0.21 and an R_{free} factor of 0.22 was obtained, which consisted of 240 residues and 272 water molecules. We modeled Zn^{2+} into the density and the B-factor of Zn^{2+} has been refined to 26. Crystallographic statistics showed the quality of the overall structure was very good. The N-terminal His-tag fragment was missed in the electron density map

TABLE 1
Data collection, phasing, and refinement statistics for MDMPI and H52A structures

	Native	Br-MDMPI	H52A
Data collection			
Wavelength (Å)	1.5418	0.92 (*peak*)	1.5418
Space group	$P3_221$	$P3_221$	$P3_221$
Cell dimensions			
a, *b*, *c* (Å)	67.3, 67.3, 128.2	67.1, 67.1, 128.1	66.6, 66.6, 129.4
a, *b*, *g* (°)	90.0, 90.0, 120.0	90.0, 90.0, 120.0	90.0, 90.0, 120.0
Resolution (Å)	1.75	1.95	2.05
R_{merge} (%)	4.4 (44.2)	6.9 (47.8)	10.1 (42.3)
I/σ	47.5 (5.7)	49.9 (8.5)	24.3 (7.8)
Completeness (%)	100.0 (99.9)	100.0 (100.0)	100.0 (99.9)
Refinement			
Non-hydrogen atoms	2146		2148
Protein	240		240
Water	272		274
R_{work} (%)	20.9		19.9
R_{free} (%)	21.9		22.2
B-Factors (Å^2)			
Protein	24.1		25.0
Water	30.2		30.5
Root mean square deviation from ideality			
Bond lengths (Å)	0.005		0.006
Bond angles (degree)	1.27		1.24
Ramachandran analysis (%)			
Most-favored regions (%)	96.6		96.2
Additional favored regions (%)	2.9		3.4
Generously allowed regions (%)	0.5		0.5

due to its location on the molecule surface, and the C-terminal residue 241 was also missed.

The structure of mutant H52A was solved by molecular replacement with MolRep (17) using the MDMPI wild type structure as a search model. After several cycles of refinement and model rebuilding, a final model with an *R*-factor of 0.20 and an R_{free}-factor of 0.22 was obtained.

A structure appraisal of the final model of MDMPI and H52A using PROCHECK (18) indicated that the main-chain torsion angles for both molecules corresponded well with allowed values (96.6% in the most favored regions of the Ramachandran plot of MDMPI and 96.2% in the most favored regions of H52A). A summary of the refinement statistics is given in Table 1.

X-ray Fluorescence Scan Analysis—To determine what kind of metal ion binds to the protein, fluorescence scan analysis of the same crystal used in data collection was performed at beamline, Photon Factory (Tsukuba, Japan). The wavelength ranges of the experiments were selected near the K-edge of Zn^{2+}, Ni^{2+}, Cu^{2+}, Mn^{2+}, Fe^{3+}, and Ca^{2+}, respectively.

Site-directed Mutagenesis of MDMPI and Enzyme Activity Assay—Fourteen mutants (supplemental Table S1) of MDMPI (W44A, H48A, H52A, N56A, C61A, Y76A, S78A, R82A, E85A, R141A, E144A, H148A, D151A, and R222A) were constructed according to the method described by Sambrook *et al.* (19). Primers used for generation of these mutants are provided in supplemental Table S2. Screening for mutants was conducted through enzymatic activity assays, and subsequently the mutations were confirmed by DNA sequencing. MDMPI activity was determined according to Feng *et al.* (9).

Protein Data Bank Accession Numbers—The coordinates and structure factors for MDMPI wild type and mutant H52A have been deposited in the RCSB Protein Data Bank under the accession numbers of 2NSF and 2NSG, respectively.

RESULTS AND DISCUSSION

Overall Structure of the MDMPI—The MDMPI of *C. glutamicum* was purified from recombinant *E. coli* and its crystal structure was resolved at 1.75 Å. The MDMPI is a monomer and belongs to α/β folding type (Figs. 2*B* and Fig. 3). Two domains were clearly observed: An N-terminal domain largely composed of α-helices and a C-terminal domain characterized by shorter stretches of α-helices and β-sheets. The core of the N-terminal domain consists of five long (≈20 residues) α-helices (α1, α2, α3, α4, and α5). Also included in the core domain is a metal ion (Fig. 3). The C-terminal domain shows a novel fold with the pattern of $\alpha\beta\alpha\beta\beta\alpha$ fold, which contains three long loops, three α-helices (α7, α8, and α9), and three β-strands (β3, β4, and β5). It is noteworthy that 42% of the amino acid residues in the C-terminal domain are located at the three long loops, with the longest loop containing 20 residues (residues 221–241) and are not part of the core C-terminal domain structure (Fig. 3).

The C-terminal Domain Represents a Novel Folding Pattern and Is Necessary for Enzymatic Activity—The folding topology of the C-terminal domain of MDMPI is novel. Structural similarity searches of MDMPI C-terminal domain utilizing the DALI server (20) showed few matches with significant Z score and small root mean square deviation values. The best match was a putative sterol carrier protein (PDB code 1WFR) with Z value of 3.0. The 67 residues of this protein share 15% sequence identity with the C-terminal domain of MDMPI and can be superimposed to this domain with a root mean square deviation of 3.3 Å.

The C-terminal domain is necessary for the enzyme activity and structural stability. When the C-terminal domain was deleted, the truncated MDMPI did not show any enzyme activity (Table 2) and existed as inclusion bodies in *E. coli* cells (data not shown). Furthermore, site-directed mutagenesis revealed

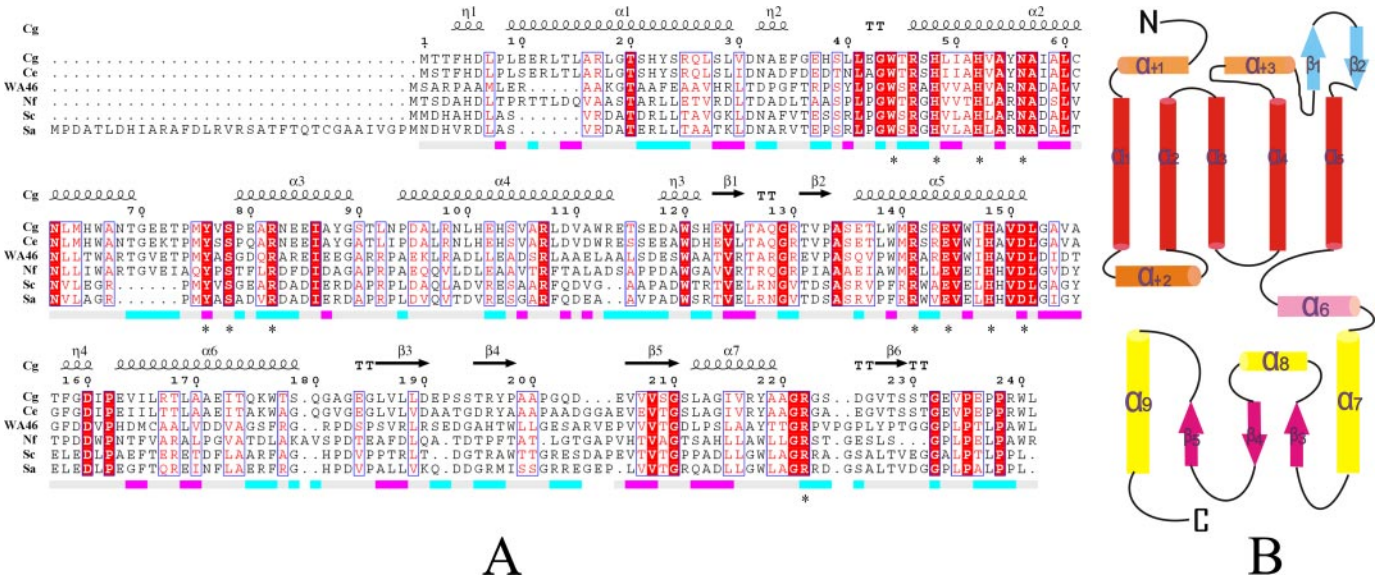

FIGURE 2. **Alignment of MDMPI from *C. glutamicum* and its homologous proteins (*A*) and topology of MDMPI (*B*).** Conserved amino acid residues are highlighted by *red*, including the metal-binding residues (His^{52}, Glu^{144}, and His^{148}) and residues for structure stability (Gly^{43}, Asn^{151}, Pro^{162}, Gly^{210}, Arg^{222}, Gly^{221}, Gly^{232}, Pro^{234}, and Pro^{238}). Amino acid residues that were mutated for generation of mutant MDMPIs in this study are indicated by *asterisk*. The sequence alignment was carried out with the EBI server ClustalW (23) and represented by ESPript (24). The abbreviations are as follows: *Cg*, *C. glutamicum*; *Ce*, *Corynebacterium efficiens*; *WA46*, *Streptomyces* sp. strain WA46; *Nf*, *Nocardia farcinica*; *Sc*, *S. coelicolor*; *Sa*, *S. avermitilis*.

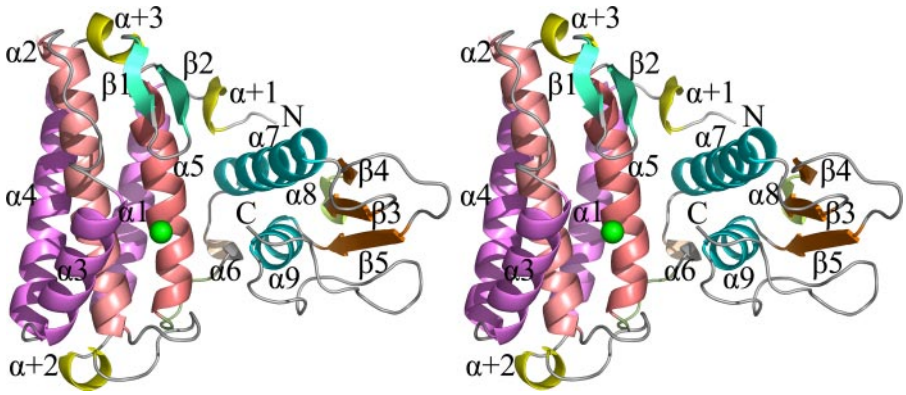

FIGURE 3. **Stereo view of the overall structure of MDMPI.** The overall structure of MDMPI consists of two domains that are connected by two loops and one α-helix (α6). In the N-terminal domain (residues 1–152), the five long α-helices (α1 to α5), which form the core part, are shown in *purple* and *pink*, and the metal ion is shown in *green*, short α-helices (α + 1, α + 2, and α + 3) are shown in *yellow*, and β-sheets (β1 and β2) are shown in *blue*. The C-terminal domain (residues 163–241) includes helices α7 and α9, a three-strand mixed β-sheet (β3, β4, and β5), which is connected by a shorter helix α8. The C-terminal domain consisted of two subdomains. The α-helices subdomain includes two α-helices (α7 and α9), and the other subdomain includes three β-sheets (β3, β4, and β5) and α8. These two subdomains are connected by three loops. A long loop (residues 221–241) is located at the terminal of the C-terminal domain. The image was created by PyMol.

The MDMPI Is a Metal-dependent Protein and Contains a Metal-binding Motif, His^{52}-Glu^{144}-His^{148}—Structural analysis revealed that MDMPI is a metal-dependent protein with the metal binding site located in the N-terminal domain. The metal atom is coordinated by His^{52} (NE2), Glu^{144} (OE1), His^{148} (NE2), two water molecules and one glycerol molecule (Fig. 5*A*). The x-ray fluorescence scan gave clear absorption jump at the spectrum over K-edge of Zn^{2+} and Ni^{2+} (data not shown), which demonstrated that this was a mixture of Zn^{2+} and Ni^{2+}. Coordination of Zn^{2+} and Ni^{2+} indicated that either could be coordinated in a tetragonal bipyramidal geometry (21). Since in the whole expression and purification course, we did not add any zinc-containing reagent, it suggested that Zn^{2+} was integrated into the metal-ion binding site *in vivo*. In addition, previous enzyme activity assays showed that Zn^{2+} (1 mM) stimulated isomerase activity up to 121%, while Ni^{2+} (1 mM) did not affect activity (9). Therefore, it is deduced that the natural MDMPI contains Zn^{2+} ion instead of Ni^{2+} ion. It is further deduced that Zn^{2+} was partially replaced by Ni^{2+} during purification of MDMPI with a nickel-affinity chromatography.

The contribution of the three conserved residues, namely His^{52}, Glu^{144}, and His^{148}, to the binding of metal atom was examined by individual mutation of each amino acid residue. Enzyme activity assays indicated that all mutants (H52A,

that a conserved Arg^{222} residue at the C-terminal domain was necessary for MDMPI activity. When this Arg^{222} residue was mutated into Ala^{222} residue, the resulting mutant R222A did not show any enzymatic activity. Structural analysis indicated that the side chain of Arg^{222} (NH1) at the C-terminal domain interacted with Asp^{151} (OD2) of the N-terminal domain through a salt bridge (Fig. 4). These two amino acid residues (Arg^{222} and Asp^{151}) are highly conserved among the protein family (Fig. 2*A*). Replacement of either of them with Ala residue resulted in complete loss of enzyme activity. Thus, it is proposed that the interaction between these two residues is vital to enzyme activity and structure stability.

TABLE 2
Determination of MDMPI activity from various MDMPIs

MDMPI wild type or mutants	MDMPI activity[a]
	%
Wild type	100
N-domain of MDMPI	0
W44A	0
H48A	100
H52A	0
N56A	0
C61A	100
Y76A	0
S78A	7
R82A	30
E85A	100
R141A	0
E144A	0
H148A	0
A151A	0
R222A	0

[a] The activity was determined from recombinant *E. coli* cells that harbor each plasmid (for details, please refer to supplemental Tables S1 and S2) and was induced by isopropyl-1-thio-β-D-galactopyranoside. The wild type MDMPI activity was calculated as 100%.

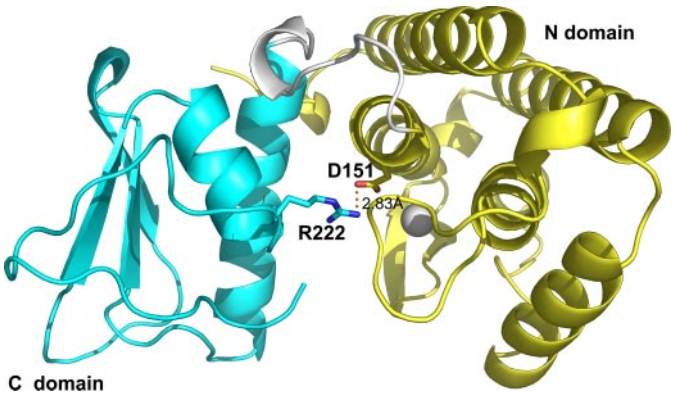

FIGURE 4. **The side chain of Arg^{222} (NH1) at the C-terminal domain interacts with Asp^{151} (OD2) of the N-terminal domain through a salt bridge.** The N-terminal domain is shown in *yellow*, C-terminal domain in *cyan*, and interdomain coil in *gray*. Asp^{151} and Arg^{222} are represented in *stick model* (carbon atoms are colored the same as the domain they locate at) and the metal ion by a *sphere* (*gray*). Salt bridge is shown by *dashed line*. The figure was created by PyMol.

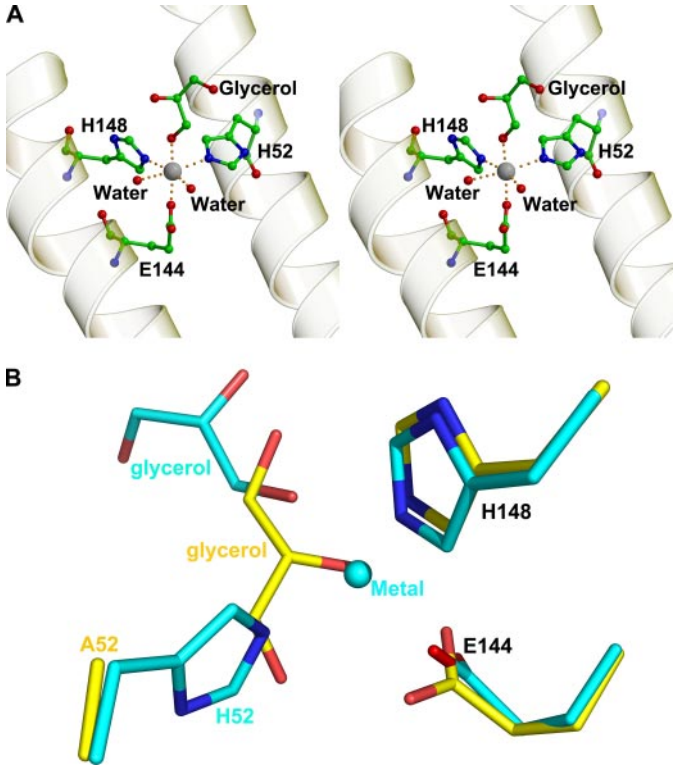

FIGURE 5. **Metal binding site of MDMPI.** *A*, stereo view of the metal binding site of wild MDMPI. Amino acid residues, glycerol, and water are shown in *ball-and-stick model*, and the metal atom is shown as a Corey-Pauling-Koltun model (*gray*). The metal binding site of MDMPI is comprised of His^{52} (NE2), Glu^{144} (OE1), His^{148} (NE2), two water molecules, and one glycerol. The His^{52} is located at the α2 helix, and the Glu^{144} and His^{148} both are located at α5 helix. This figure was created by Molscript (25) and Raster3D (26). *B*, the superimposition of the metal binding regions of the native (carbon atoms and the metal atom in cyan) and mutant (carbon atoms in *yellow*) MDMPI molecules. The position of metal atom at native MDMPI was replaced by one glycerol moiety in mutant H52A. The image was created by PyMol.

E144A, and H148A) were inactive. Moreover, the crystal structure of mutant H52A at resolution of 2.05Å revealed that there was no metal ion bound to the protein (although nickel-affinity chromatography was used in the purification process). The metal atom position at the native MDMPI molecule was occupied by one glycerol moiety (Fig. 5*B*). Compared with the native MDMPI, the mutant MDMPI (H52A) has the following structural changes: 1) the main chain of the loop (amino acid residues 36–45) moved toward the inner; 2) the side chain of Trp^{44} at the loop is much closer to the former metal binding site; 3) the side chain of Glu^{144} had double conformations; and 4) conformational change took place at the side chain of Arg^{82} (Fig. 6). Probably it is the absence of the metal ion that resulted in the significant conformation change around the proposed metal binding region.

Previously, it was proposed that MDMPI represents a novel family of proteins (9), but the structures of this novel family were unknown. According to sequence alignment, the metal binding site, namely residues His^{52}-Glu^{144}-His^{148}, are highly conserved throughout the whole family (Fig. 2*A*), and these binding residues are located in the surface pocket between the α2 (His^{52}) and α5 (Glu^{144} and His^{148}) in N-terminal domain (Fig. 5*A*).

Biochemical and Structural Identification of Catalytic Center—In total fourteen amino acid residues were targeted for mutation (Table 2), according to sequence alignment and the above structure analysis. Some mutant MDMPIs such as H52A, E144A, H148A, D151A, and R222A that completely (100%) lost enzymatic activity were described above. The other mutant MDMPIs include three (H48A, C61A, E85A) that did not lose activity, two that showed significant loss of activity (S78A, 7%; R82A, 30%; activity remained), and four (Y76A, R141A, W44A, N56A) that demonstrated a complete loss of activity (Table 2). Structure modeling indicated that Tyr^{76}, Arg^{82}, Ser^{78}, Arg^{141}, Trp^{44}, and Asn^{56} are located at the metal-binding region. Moreover, eight of these amino acid residues, including His^{52}, Trp^{44}, Asn^{56}, Tyr^{76}, Arg^{82}, Arg^{141}, Glu^{144}, and His^{148}, formed a surface pocket (Fig. 7). The metal ion (Zn^{2+}) and its binding site (His^{52}, Glu^{144}, and His^{148}) are located at the bottom of the surface pocket. Thus, it is proposed that these highly conserved sites (Trp^{44}, Asn^{56}, Tyr^{76}, Arg^{82}, and Arg^{141}) that surrounding the metal binding site provides the hydrophilic environment for MDMPI catalysis. The surface pocket including the metal atom

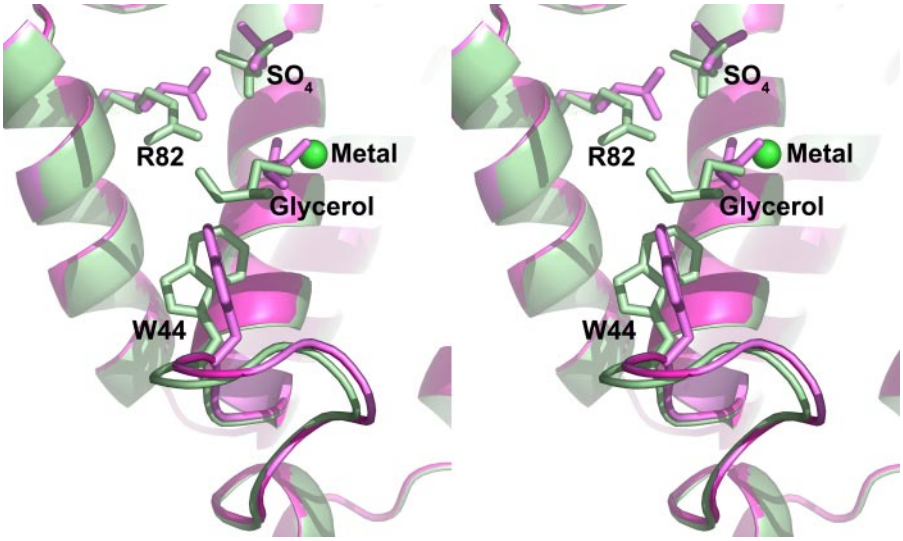

FIGURE 6. **The stereo view of the conformation differences in the putative active pocket between the wild type and the mutant (H52A) MDMPI.** Mutant H52A is shown in *purple* and native MDMPI in *green*. Conformation differences were found at the side chains of Arg^{82} and Trp^{44}. In H52A the metal ion was missing and a glycerol occupied the position of the metal ion, and the location of SO_4^{2-} also changed. Furthermore, there is no obvious conformation changes observed, when compared with that of the wild type. The image was created by PyMol.

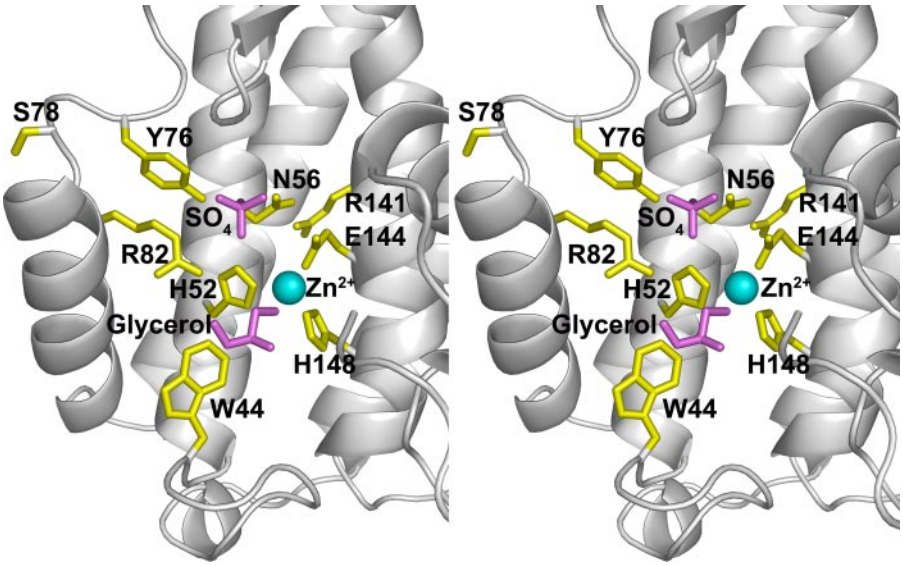

FIGURE 7. **The stereo view of the structural elements involved in the putative active pocket.** The conserved metal binding residues (His^{52}, Glu^{144}, and His^{148}) and other conserved residues (Asn^{56}, Tyr^{76}, Ser^{78}, Arg^{82}, Arg^{141}, and Trp^{44}) form the putative active pocket. Residues are shown in *yellow* (*stick*), the metal ion (Zn^{2+}) is shown in *cyan* (*sphere*), and the SO_4^{2-} ion and glycerol in *purple* (*stick*). The image was created by PyMol.

(Zn^{2+}) and the MSH moiety further formed the potential catalytic center.

Sulfate Ion in the Catalytic Center and Proposed Process for MDMPI-catalyzing Isomerization—A tetrahedral density was observed at this surface pocket. This density was molded as a sulfate ion (Fig. 7). The sulfate ion interacted with Tyr^{76} and Asn^{56} and was located near Arg^{82}. These three amino acid residues are conservative in the whole family (Fig. 2*A*) and are necessary for enzymatic activities, as demonstrated by mutagenesis of these amino acid residues resulting complete loss of enzymatic activity (Table 2). Interestingly, a sulfate ion was also observed in the active site (a deep cavity) of the human GSH-dependent maleylacetoacetate isomerase, and this sulfate ion was proposed to mimicking substrate (maleylacetoacetate) binding (22).

Although the catalytic mechanism of MDMPI is still not clear, this and previous studies have revealed several key molecular elements that are necessary for catalysis, including the metal ion (Zn^{2+}) and its surrounding amino acid residues (His^{52}, Glu^{144}, and His^{148}), and the –SH group of the MSH molecule (9). Here, a preliminary and hypothetical process is proposed for description of the MDMPI-catalyzed isomerization (Fig. 1): isomerization of maleylpyruvate is initiated by the attack of –SH of the mycothiol on the α-carbon of the maleylpyruvate molecule, which is catalyzed by the MDMPI (most probably by the Zn^{2+} ion on the enzyme). This attack results in the formation of MSH-maleylpyruvate conjugate (Fig. 1, step *I*). Upon conjugation, the resulting single bond would be freely to rotate (Fig. 1, step *II*). Finally, the MSH moiety is released and the product (fumarylpyruvate) is generated (Fig. 1, step III). Although this proposed mechanism is similar to that proposed for the GSH-dependent maleylacetoacetate isomerase from humans (22), some sharply different properties between MDMPI and GSH-dependent maleylacetoacetate were observed. The MDMPI is a metalloprotein but the GSH-dependent maleylacetoacetate isomerase is not; the latter belongs to a group of enzymes named zeta class glutathione transferase that catalyze reductive dehalogenation of α-hologenated acids (22), but this property was not observed for the MDMPI from *C. glutamicum*. Currently, works on characterization of more MDMPIs from different bacteria and on details of the catalytic mechanism of MDMPI are in progress.

Acknowledgments—We are grateful to Rui-Fang Wang for protein purification, Yi Han at the Institute of Biophysics (Chinese Academy of Sciences), Yu-Hui Dong and Peng Liu at the Institute of High Energy Physics (Chinese Academy of Sciences) for data collection, and N. Sakabe and A. Iida of the Photon Factory (Tsukuba, Japan) for x-ray fluorescence scanning.

REFERENCES

1. Buchmeier, N. A., Newton, G. L., Koledin, T., and Fahey, R. C. (2003) *Mol. Microbiol.* **47,** 1723–1732
2. Newton, G. L., Ta, P., Bzymek, K. P., and Fahey, R. C. (2006) *J. Biol. Chem.* **281,** 33910–33920
3. Buchmeier, N. A., Newton, G. L., and Fahey, R. C. (2006) *J. Bacteriol.* **188,** 6245–6252
4. Spies, H. S., and Steenkamp, D. J. (1994) *Eur. J. Biochem.* **224,** 203–213
5. Newton, G. L., Arnold, K., Price, M. S., Sherrill, C., Delcardayre, S. B., Aharonowitz, Y., Cohen, G., Davies, J., Fahey, R. C., and Davis, C. (1996) *J. Bacteriol.* **178,** 1990–1995
6. Newton, G. L., and Fahey, R. C. (2002) *Arch. Microbiol.* **178,** 388–394
7. Newton, G. L., Unson, M. D., Anderberg, S. J., Aguilera, J. A., Oh, N. N., delCardayre, S. B., Av-Gay, Y., and Fahey, R. C. (1999) *Biochem. Biophys. Res. Commun.* **255,** 239–244
8. Rawat, M., Newton, G. L., Ko, M., Martinez, G. J., Fahey, R. C., and Av-Gay, Y. (2002) *Antimicrob. Agents Chemother.* **46,** 3348–3355
9. Feng, J., Che, Y., Milse, J., Yin, Y. J., Liu, L., Rueckert, C., Shen, X. H., Qi, S. W., Kalinowski, J., and Liu, S. J. (2006) *J. Biol. Chem.* **281,** 10778–10785
10. Shen, X. H., Jiang, C. Y., Huang, Y., Liu, Z. P., and Liu, S. J. (2005) *Appl. Environ. Microbiol.* **71,** 3442–3452
11. Otwinowski, Z., and Minor, W. (1997) *Methods Enzymol.* **276,** 307–326
12. Adams, P. D., Grosse-Kunstleve, R. W., Hung, L. W., Ioerger, T. R., McCoy, A. J., Moriarty, N. W., Read, R. J., Sacchettini, J. C., Sauter, N. K., and Terwilliger, T. C. (2002) *Acta Crystallogr. Sect. D Biol. Crystallogr.* **58,** 1948–1954
13. Adams, P. D., Gopal, K., Grosse-Kunstleve, R. W., Hung, L. W., Ioerger, T. R., McCoy, A. J., Moriarty, N. W., Pai, R. K., Read, R. J., Romo, T. D., Sacchettini, J. C., Sauter, N. K., Storoni, L. C., and Terwilliger, T. C. (2004) *J. Synchrotron Radiat.* **11,** 53–55
14. Lamzin, V. S., and Wilson, K. S. (1993) *Acta Crystallogr. Sect. D Biol. Crystallogr.* **49,** 129–149
15. Perrakis, A., Sixma, T. K., Wilson, K. S., and Lamzin, V. S. (1997) *Acta Crystallogr. Sect. D Biol. Crystallogr.* **53,** 448–455
16. Brunger, A. T., Adams, P. D., Clore, G. M., DeLano, W. L., Gros, P., Grosse-Kunstleve, R. W., Jiang, J. S., Kuszewski, J., Nilges, M., Pannu, N. S., Read, R. J., Rice, L. M., Simonson, T., and Warren, G. L. (1998) *Acta Crystallogr. Sect. D Biol. Crystallogr.* **54,** 905–921
17. Vagin, A., and Teplyakov, A. (1997) *J. Appl. Crystallogr.* **30,** 1022–1025
18. Laskowski, R. A., MacArthur, M. W., Moss, D. S., and Thornton, J. M. (1993) *J. Appl. Crystallogr.* **26,** 283–291
19. Sambrook, J., Russell, D. W., and Maniatis, T. (1989) *Molecular Cloning, A Laboratory Manual*, Cold Spring Harbor Laboratory Press, Cold Spring Harbor, NY
20. Holm, L., and Sander, C. (1995) *Trends Biochem. Sci.* **20,** 478–480
21. Auld, D. S. (2001) *Biometals* **14,** 271–313
22. Polekhina, G., Board, P. G., Blackburn, A. C., and Parker, M. W. (2001) *Biochemistry* **40,** 1567–1576
23. Chenna, R., Sugawara, H., Koike, T., Lopez, R., Gibson, T. J., Higgins, D. G., and Thompson, J. D. (2003) *Nucleic Acids Res.* **31,** 3497–3500
24. Gouet, P., Courcelle, E., Stuart, D. I., and Metoz, F. (1999) *Bioinformatics* **15,** 305–308
25. Kraulis, P. J. (1991) *J. Appl. Crystallogr.* **24,** 946–950
26. Merritt, E. A., and Murphy, M. E. (1994) *Acta Crystallogr. Sect. D Biol. Crystallogr.* **50,** 869–873